Materials Today Bio 13 (2022) 100179

Contents lists available at ScienceDirect

Materials Today Bio

journal homepage: www.journals.elsevier.com/materials-today-bio

Functional amyloid-chitin hybrid ink coupled with flexible fabrication approaches for diverse macro and micro-structures

Shicao Wei [a], Yingfeng Li [a], Ke Li [a], Anqi Kang [a], Siyu Zhang [a], Teng Feng [b], Hui Zhang [b], Chao Zhong [a,c,d,*]

[a] Materials and Physical Biology Division, School of Physical Science and Technology, ShanghaiTech University, Shanghai, 201210, China
[b] School of Life Science and Technology, ShanghaiTech University, Shanghai, 201210, China
[c] Center for Materials Synthetic Biology, Shenzhen Institute of Synthetic Biology, Shenzhen Institute of Advanced Technology, Chinese Academy of Sciences, Shenzhen, 518055, China
[d] CAS Key Laboratory of Quantitative Engineering Biology, Shenzhen Institute of Synthetic Biology, Shenzhen Institute of Advanced Technology, Chinese Academy of Sciences, Shenzhen, China

ARTICLE INFO

Keywords:
Composites
Bio-fabrication
Functional amyloid
Polysaccharide
Protein Self-assembly

ABSTRACT

The precise fabrication of artificially designed molecular complexes into ordered structures resembling their natural counterparts would find broad applications but remains a major challenge in the field. Here we genetically design chitin-binding domain (CBD)-containing amyloid proteins, and rationally fabricate well-ordered CBD-containing functional amyloid-chitin complex structures by coupling a top-down manufacturing process with a bottom-up self-assembly. Our fabrication approach starts with the dissolution of both CBD-containing functional amyloid and chitin in hexafluoroisopropanol (HFIP) to make a hybrid ink. This hybrid ink platform, coupled with multiple fabrication methods including airbrushing, electrospinning and soft-lithography, produces a series of unique freestanding structures. The structural features of the products, such as the ability to direct the light path and mimicking of the extracellular matrix enable applications in functional light gratings and cell culture, respectively. Further genetic engineering of the protein component allowed tunable functionalization of these materials, including nanoparticle immobilization and protein conjugation, resulting in broad applications in electronic devices and enzyme immobilization. Our technological platform can drive new advances in bio-catalysis, tissue engineering, biomedicine, photonics and electronics.

1. Introduction

Biological materials have attracted growing interest among materials scientists [1,2]. Natural structures in animals and plants provide both inspiration and building blocks for development of new materials [3–5]. Biologically derived components are increasingly explored as building blocks for new sustainable materials [6]. In nature, these building blocks usually take a composite form, and function in a complementary manner [7], such as the protein-polysaccharide exoskeleton in crustacea [8] and cellulose-lignin cell wall structure of lignocellulosic plants [9]. Their structural features and primary functionality have been extensively studied [6,7,11], and a series of biomimetic protein-polysaccharide composite materials have been developed. A common approach, which has been applied in the areas of biocatalysis [12], biophotonics [13], bioelectronics [14], tissue engineering [15] and regenerative medicine [16], is to use a functional protein and a common polysaccharide [17–24]. However, these studies mainly focus on developing biomimetic composites for a specific purpose, such as improving interaction between components or generating interesting structures or performing a simple functionality. Here we seek to integrate these functions by developing a hybrid ink system that consists of two components: the genetically engineerable amyloid protein CsgA and the polysaccharide chitin (β-chitin).

CsgA, the structural monomer from *E. coli* biofilms [25] is an ideal genetically engineerable protein [26,67–69], which can be functionalized with diverse heterologous peptides (functional peptides) [27,28] or domains (such as domains that improving interaction between the components). At the same time, its outstanding mechanical properties and high physiochemical stability [29] make it suitable for applications in material science [57,66]. Importantly, a solvent-assisted renaturation

* Corresponding author. Materials and Physical Biology Division, School of Physical Science and Technology, ShanghaiTech University, Shanghai, 201210, China.
E-mail address: chao.zhong@siat.ac.cn (C. Zhong).

https://doi.org/10.1016/j.mtbio.2021.100179
Received 1 October 2021; Received in revised form 29 November 2021; Accepted 1 December 2021
Available online 2 December 2021

fabrication method has been developed for CsgA to overcome the difficulties in handling the amyloid fibers that arise due to spontaneous aggregation [30]. In the case of β-chitin, many studies have explored the function and structural properties of this amazing biopolymer [31]. In addition, the concept of a chitin ink or precursor solution has already been developed to ease solution processing [32] and many subtle structures have been fabricated using this natural material [14,33–35]. Based on these studies and inspired by the bio-ink concept developed in 3D-printing and biomedicine [36–38], we use the same solvent, hexafluoro-2-propanol (HFIP) to dissolve the two components to create a hybrid ink. We then used a methanol-assisted curing technology [39], from macro- to nanoscale, and employed airbrushing, electrospinning and lithography to generate a broad variety of self-assembled amyloid-chitin complexes with pre-defined ordered structures (Fig. 1). Notably, genetic engineering of the protein component allowed further functionalization of these materials, including nanoparticle immobilization and protein conjugation, finding applications in electronic devices and enzymatic catalysis.

2. Materials and methods

2.1. Materials

LB broth (MD bio), imidazole (99%, Energy Chemical), carbenicillin disodium (carb, USP, Macklin), isopropyl-β-D-thiogalactopyranoside (IPTG, Ultrapure, Life Science), guanidine hydrochloride (GdnHCl, AR, Sinopharm), Phosphate Buffered Saline (PBS, ABCONE), sodium hydroxide (NaOH, AR, Sinopharm), hydrochloric acid (HCl, GR, General Reagent), sodium dodecylsulfate (SDS, Beyotime) 1,1,1,3,3,3-hexafluoro-2 propanol (HFIP, SP, Aldrich), polydimethylsiloxane (PDMS, SYLGARD184Dow Corning), methanol (AR, Aldrich), ethanol (SP, Macklin), isopropyl alcohol (SP, Xilong Scientific), polyvinyl alcohol (PVA, 3000 Da, BR, Sangon Biotech).

2.2. Plasmid construction

Target gene sequences were synthesized and further amplified by PCR and then were cleaved by restriction enzymes Nde I and Xho I (Fermentas Fast Digest) for 45 min at 37 °C. The prepared fragments and the Nde I and Xho I digested plasmid pET-22b were mixed and incubated with appropriate amount of Gibson Assembly Master Mix (NEB) for 1 h at 50 °C, then transformed into BL21 (DE3) *E. coli* competent cells (TransGen Biotech). The *E. coli* strains were then smeared to the surface of LB media plates containing antibiotics to select transformants. All constructs were sequenced and verified by Genewiz at Suzhou.

2.3. Protein expression, purification and identification

For the recombinant amyloid proteins, bacterial seed cultures were cultured overnight in 5 ml LB at 37 °C, 220 rpm. An additional 1 L of room-temperature LB was added to the culture. When the culture was grown to OD_{600} 0.8, IPTG was added with a final concentration of 1 mM. The culture was then incubated for 60 min at 37 °C followed by centrifugation for 10 min at 4000 g at room temperature. The cell pellets (5 g) were then lysed in 50 ml GdnHCl (in PBS buffer) for 48 h at 4 °C. Supernatants of the lysates were collected at 12,000 g for 40 min before loading onto a His-Select Ni-NTA (Genscript) column. The column was washed with PBS buffer and 20 mM imidazole PBS buffer, then eluted with 500 mM imidazole PBS buffer. For the recombinant enzyme and fluorescent proteins, the cell pellets were lysed 2–3 times by sonic disruption at ~60% power with on/off intervals of 5s. The proteins were then purified using the same protocol for purification of the recombinant amyloid proteins described abvove.

Polyacrylamide gel electrophoresis (SDS-PAGE) and western-blot analysis were carried out to confirm the purified proteins and their molecular weights. Briefly, fresh protein extract mixed with loading buffer was loaded on a minigel (Life Technologies) and run alongside a standard protein ladder (Life Technologies) at 168 V for 40 min using Nupage MES running buffer (NOVEX). For the SDS-PAGE the gels were stained with

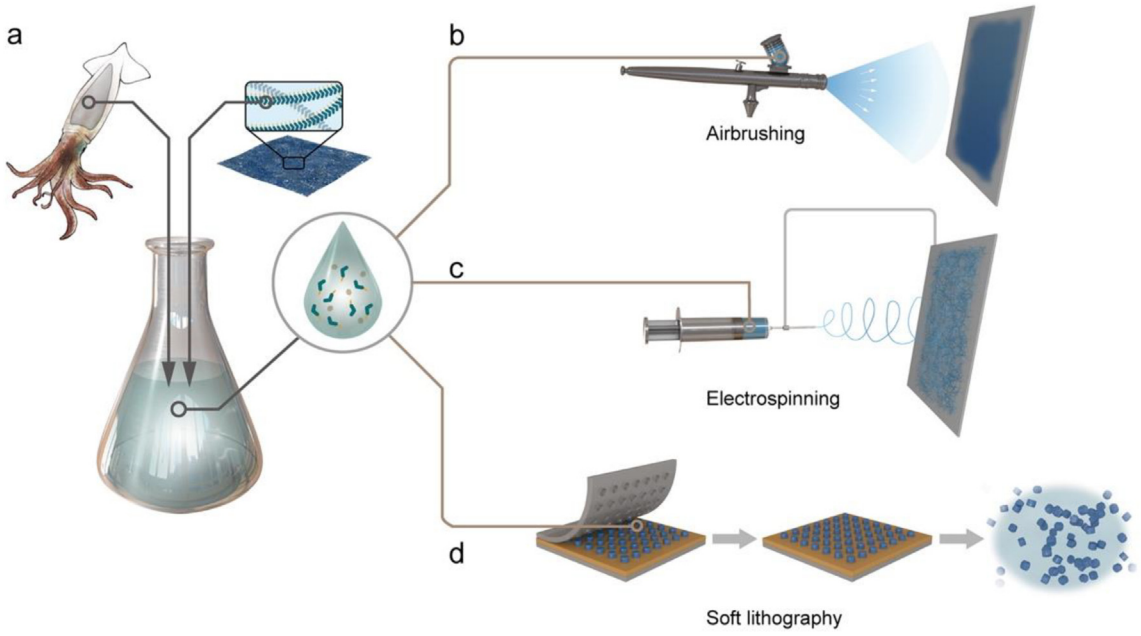

Fig. 1. Schematic illustration of the amyloid-chitin hybrid ink and applications of the hybrid ink for multi-scale structure fabrications across several length scales by coupling with diverse fabrication technologies. (a) The chitin derived from squid pens and amyloid fibers derived from genetically engineered biofilms are first dissolved in HFIP to obtain a chitin-amyloid hybrid ink. (b) The hybrid ink can be applied by airbrushing to produce a macro-scale thin film structure. (c) The hybrid ink can be combined with an electrospinning process to produce a dense fibrous web. (d) The hybrid ink can be coupled with soft lithography to produce freestanding micro-structures.

Coomassie Blue solution (Amresco) for 1 h, and after destaining, were washed twice for 1 h with a solution of methanol, acetic acid and water (4:1:5 vol ratio). The gels were then imaged using a Bio-Rad ChemiDoc MP system. For the Western-blot analysis, protein samples were blotted onto polyvinylidenedifluoride membranes using the iBlot system (Invitrogen). The membranes were then blocked with 40 ml 20% (m/v) milk solution for 1 h and washed three times with 10 ml 1 × TBST for 10 min. After that, membranes were incubated with 30 ml anti-His antibodies diluted to 1:5000 for 1 h and washed three times with 10 ml 1 × TBST for 10 min. They were then incubated with 30 ml secondary anti-mouse antibodies diluted to 1:5000 for 1 h. After treatment with 1 × TBST, the membranes were imaged using a Bio-Rad ChemiDoc MP system.

2.4. Chitin purification

The β-Chitin samples used in our experiment were purified from squid pen (collected from Yantai, Shandong province, China), with detailed protocol provided below. First, the squid pens were smashed with a mortar, and then soaked in 1 M HCl for 12 h followed by treatment with 1 M NaOH for 12 h. The last two steps were repeated five times. The residual solid material was then decolored by immersing it in 0.5% $NaClO_2$, and then the pH was adjusted to 5 using acetic acid. This suspension was heated for 2 h at 70 °C. The purified β-Chitin solids were obtained by centrifugation and stored at 4 °C.

2.5. The fabrication methods

Because HFIP is a corrosive and volatile solvent, the bioink preparing process and the composite materials fabrication were strictly carried out under appropriate operation conditions, either in a fume hood or under a ventilated environment.

2.5.1. Airbrushing

A commercially available external mix airbrush was used (Ustar HD130) to spray chitin ink onto PDMS based glass slide template. In the current geometry (10 cm nozzle-substrate distance, spray angle 15°) ≈5 cm^2 area was painted to get a film (15 cm^2 for the thickness-time relationship) using a 2 mg/ml composite ink at 0.02 ml/s airflow (nitrogen as the driving gas) and the process was interrupted once every minute to protect the muzzle from blocking. The films made by this method were then immersed in the methanol bath for 6 h to recover their amyloid structures.

2.5.2. Soft lithography

Fabrication of patterned PDMS stamps: PDMS stamps were fabricated by casting mixed pre-polymer and curing agent using patterned silicon as the initial mold. SYLGARD 184 was used with a 10:1 ratio to polymer base curing agent. After pouring over the master followed by vacuum degassing, the PDMS was cured at 80 °C for 3 h and lifted out. After being cured, PDMS was cut into the desired defined shape with a razor blade in the size of 1cmx1cm.

Patterned structures fabricated via micro-transfer molding and curing process: forty microliter hybrid ink solution (2 mg/ml) was added dropwise to the surface of a cleaned glass slide using a pipette. PDMS stamps were gently placed on the glass slide to completely cover the solution, followed by incubation for 1 s to allow complete diffusion. The PDMS stamps were then immediately transferred to a clean substrate using a cleaned tweezer and incubated for 30 min. After peeling off the PDMS stamps, the samples were immersed in methanol solution (100%) overnight to obtain a cured structure.

Preparation of self-supporting gratings: the hybrid ink solution was added dropwise to the surface of a PDMS stamp, then the ink was dried to form a film.

Preparation of self-supporting patterns: 1 mL PVA (5%) aqueous solution was cast onto a glass substrate to form a uniform sacrificial layer. The patterns were formed on these sacrificial layers. The self-supporting patterns were prepared after dissolving the sacrificial layer in copious amount of ddH_2O.

2.5.3. Electrospinning

The hybrid ink was loaded into 5 ml plastic syringes (medical injection syringe, Golden Dragon Chang Zhou) equipped with a blunt 21-gauge (21 g) needles. Then the syringe was loaded on an electrospinning device (Kang Yongle Beijing Science and Technology Development Limited Company). Fibers were collected onto aluminum foil sheets which were attached to low voltage power using a delivery rate of 0.05 ml/min. Different needle gauges (19 g and 17 g) and voltage were tested for their effects on fiber diameter. The prepared electrospinning fibers were then incubated in the methanol bath for 6 h to recover their amyloid structures.

2.6. Paraoxon-ethyl degradation

Here, PDMS based holes in a 12-orifice plate were used as the template for forming the film. About 2 ml of hybrid ink was used to form these films and then the films were incubated with the $OPH_{Spycatcher}$ protein solution at 16 °C overnight. The degradation test was carried out as follows: the composite film was reacted with 2 ml of 50 mM Paraoxon-ethyl and the absorption at 405 nm was measured using an absorption spectrometer.

2.7. Congo red staining

The protein solutions were kept at room temperature for several days, then 200 μL of 20 μg/ml protein solutions were spotted onto Protran BA83 nitrocellulose membranes (Whatman) with a dot blot manifold (Schleicher & Schuell Minifold-I Dot-Blot System). The membranes were then incubated with 40 ml of 0.002 (m/v%) Congo red solution at room temperature for 1 h. After being stained, the membranes were washed three times with ddH_2O.

2.8. Fluorescent protein conjugation

Self-supporting structures and patterns (films, porous sheet and disks) were directly deposited in a solution containing the fluorescent proteins for 60 min, and were then scooped out with the glass substrate, followed by rinsing with PBS buffer. For the electrospun fibers, the fibers were collected on glass slides in the electrospinning process and the fluorescent solution was dropped on the fiber area after the curing process.

2.9. Ni-NTA capped QDs assembly

The cured patterned electrospun fiber structures on glass substrates were exposed to a solution containing Ni-NTA decorated QDs for 1 h in the dark followed by washing with a copious amount of ddH_2O to remove loosely bounded QDs. The structures were then dried through a constant flow of N_2 gas. Synthesis and ligand exchange of QDs was carried out as previously described [40].

2.10. Cell culturing

The electrospun fibers were sterilized by ethanol and UV light, then the fiber matrix was added to the cell culture solutions. Cells were cultured in DMEN (Dulbecco's Modified Eagle medium) containing 10% FBS and antibiotics at 37 °C and 5% CO_2.

2.11. Cellular staining and cell counting

The cell viability test was performed by the Trypan blue dye method. The cell morphology including nucleus and cytoskeleton features was observed under fluorescence microscope after the cell was stained by DAPI and phalloidin.

2.12. Analytical techniques for characterization

2.12.1. Atomic force microscope

For aqueous solutions, a 200 μL droplet was directly deposited on a mica sheet for 5 h and was then washed by ddH_2O and dried with N_2. For samples in HFIP solution, a 2 μL droplet was directly deposited on a mica sheet. Samples were tested by an Asylum AR MFP-3D-Bio- Atomic force microscope.

2.12.2. X-ray fiber diffraction

A 2 μL solution of cured nanofibers (scraped from silicon substrate) was dropped by pipette between the tips of two prepared capillary tubes. Protein nanofibers were aligned along the capillary tube tips after water evaporation. The samples were finally tested with a Rigaku Micromax-007 X-ray generator equipped with an R-Axis IV++ area detector.

2.12.3. Scanning electron microscopy

Before being observed by scanning electron microscopy the samples were dehydrated using an ethanol gradient. For cell culture samples, the cells were fixed before dehydration. The samples were coated with Au for 10 s with an SBC-12 sputter coater, then imaged with JSM 7800 F Prime or JSM-6010PLUS/LA scanning electron microscope.

2.12.4. Transmission electron microscopy

QDs bound to electrospun fibers were immersed in ddH_20 and the mixture was directly deposited on a transmission electron microscope (TEM) grid (Zhongjingkeyi Technology, EM Sciences) for 5 min. Excess solution was wicked away with filter paper and the samples were rinsed with ddH_2O. All samples were negatively stained with 5 μL 2% uranyl acetate for 30s. Excess uranyl acetate was wicked off and the grid was dried for 15 min under an infrared lamp (Zhongjingkeyi Technology). TEM images were obtained on a JEM-1400plus transmission electron microscope operated at 120 kV accelerating voltage.

2.12.5. Fluorescence microscopy

Fluorescence imaging was performed on a Zeiss Z2, Leica Dmi8 or LSM 710 fluorescence microscope. The 488 nm laser was used for excitation of $GFP_{Snoopcatcher}$ while a 545 nm laser was applied to excite $mCherry_{Spycatcher}$ or red emitting QDs.

2.12.6. Stress-strain test

The stress-strain test for the composite film samples was performed on the instron 5966 (universal material testing system) equipped with a 100 N load cell, 250 N pneumatic side action tensile grips and flow rate 10 mm/min. The data were recorded for three rectangular samples (2 cm (length) x 0.5 cm (width) shape) for each material under normal room temperature and humidity. The samples were immersed in the methanol bath for 1 h to be fully cured and then, dried before the test. The samples were first fixed by the tensile grips (0.5 cm length in each grip) and straightened. The test was stopped when the film was broken.

2.12.7. Transmissibility and reflectivity test

The transmissibility and reflectivity of the film sample were analyzed on an Agilent Cary 5000 ultraviolet spectrophotometer using the transmittance and reflectivity module.

2.12.8. Quartz crystal microbalance (QCM)

QCM curves were collected using a Q-Sense Omega Autosystem. A total of 30 μL chitin ink (2 mg/ml) was deposited on Au quartz crystal with fundamental frequencies of ~5 MHz by spin coating (1000 rpm, 5 s, Polos). Protein aqueous solution was injected into the flow cell with a rate of 5 μL min^{-1}. The adsorbed protein on the crystal was then washed with PBS to remove any non-specifically bound nanofibers. Data were fitted using the Voigt model.

2.12.9. Attenuated total reflection-flourier transform infrared spectroscopy (ATR-FTIR spectroscopy)

ATR-FTIR spectra of the native, uncured and cured CsgA or $CsgA_{CBD}$ samples were recorded from 1700 to 1600 cm^{-1} using a nominal resolution of 1 cm^{-1} with Spectrum TwoTM (PerkinElmer). The native nanofiber sample from protein solutions was first collected by centrifuge of the solution at 12000 rpm and dried at room temperature. The cured nanofibers were prepared as follow: the uncured samples were immersed into the methanol solvent to allow their reassembly into amyloid structures. Then the mixture was centrifuged (12000 rpm) to collect the cured fibers and dried at room temperature before use. All of the protein nanofibers were put on the ATR crystal directly for ATR-FTIR characterization. The uncured samples were prepared by evaporation of the HFIP solvent under fume hood. The sample was then put on the ATR crystal for ATR-FTIR characterization.

2.12.10. Peak force quantitative nano mechanical AFM

The Young's modulus of protein and amyloid samples was measured using an AFM (Bruker Fast Scan) in peak force quantitative nanomechanical mode. A Derjaguin-Mueller-Toporov (DMT) model was used to determine the value of Young's modulus [41,42].

In the DMT model

$$F = \frac{4}{3}\frac{E}{(1-\mu^2)}\sqrt{R}\delta^{\frac{3}{2}}$$

where F is the force that can be acquired from the fitting force curve; E is the Young's modulus; μ is the Poisson's ratio; R is the radius of tip; δ is the indentation depth.

Sample preparation for Young's modulus measurements: For an uncured sample, 20 μL solution containing the composite samples dissolved in the HFIP solvent (0.5 mg/ml) was carefully drop-casted on a mica substrate (~1 cm^2) and dried before mechanical test. For the cured sample, 20 μL composites (in HFIP, 0.5 mg/ml) were first drop-casted on a mica substrate and dried then immersed in the methanol bath for 24 h, and dried before mechanical test.

In a specific testing process, the deflection sensitivity of cantilevers (AC160TS-R3, Olympus, k ≈ 26 N/m, ν ≈ 300 kHz) was calibrated on a mica substrate. Tip radius was measured using a tip characterizer sample (Bruker). Deformation was kept in the range of 5–10 nm. For a specific area of the sample, 256 × 256 points were tested to obtain corresponding force curves. The values of F and δ could be acquired from these force curves. The Poisson's ratio of the uncured and cured proteins was set for 0.3. The calculations of Young's modulus were performed using the system internal software. All the values of Young's modulus were exported and plotted using Origin software.

3. Results and discussion

3.1. The component design of the amyloid-chitin composite ink

To fabricate functional amyloid-polysaccharide complex structures of different length scales, we set out to rationally design multi-domain functional amyloids for selective binding of chitin nanofibers derived from squid pens. CsgA served as the backbone domain that drove the self-assembly of the constructed molecules. To allow further engineering of the protein, CsgA was fused to Spytag or Snooptag sequences, which enable the amyloid protein to be functionalized with other proteins containing the Spycatcher or Snoopcatcher sequence [43,44]. The multi-domain functional amyloids were designed to contain three domains: CsgA, the Spytag/Snooptag sequence, and the chitin binding domain. To allow interactions with chitin, the chitin binding domain (CBD) sequence was added and the C-termini were tagged with poly-histidine residues to enable purification [45]. The final functional protein module was a multi-domain amyloid fusion protein in which the Spytag/Snooptag sequence and the CBD domain followed by a His tag

were genetically engineered at the N- and C-terminus of CsgA, respectively (Spytag/Snooptag-CsgA-CBD-His). The protein design is shown schematically in Fig. 2a. These proteins, $_{Spytag}CsgA_{CBD\text{-}His}$ and $_{Snooptag}CsgA_{CBD\text{-}His}$ are hereafter referred to as SPCC and SNCC.

The functional amyloids were expressed and purified in *E. coli*, and western blot analysis was used to confirm their size (Figure S1). Morphological characterization by atom force microscopy (AFM) confirmed that the genetically engineered proteins can self-assemble into fiber structures in solution (Fig. 2b and e). The fiber diameter of SPCC and SNCC is larger than either CsgA and $CsgA_{CBD}$ (Figure S6). A Congo Red (CR) staining assay (Fig. 2c and f) revealed the amyloidogenic features of the fibers. The structural characterization by fiber-XRD diffraction confirmed a typical β-sheet diffraction pattern of the tri-domain amyloid proteins (Fig. 2d and g).

To generate the polysaccharide ink component, β-chitin was purified from squid pens and the material was desalinated and deproteinized. After preparing the two components, a hybrid ink system containing the two components dissolved in HFIP coupled with a curing process is developed and applied to create amyloid/chitin composite materials.

3.2. A hybrid ink system coupled with a curing process for composite fabrication

The hybrid ink was prepared by dissolving the amyloid components and chitin (mixing ratio 1:1) in hexafluoroisopropanol (HFIP). Here we choose HFIP as the hybrid ink solvent based on several reasons: first, although HFIP is a very harsh and relatively expensive solvent, it is a suitable solvent to dissolve both amyloid proteins and chitin and the study doesn't require a huge amount of it. Specifically, HFIP is a good hydrogen-bond-donor for both CsgA and chitin and easily dissolves these two components through hydrogen bond disruption [46], which allows their homogeneous blending in the form of a clear solution (Fig. 2i). Second, the HFIP solvent is a high volatile solvent (boiling point 59 °C) and a poor hydrogen-bond-receptor, which allows HFIP to freely evaporate under ventilated environment and the composite mixture is solvent-free after volatilization [35]. As our fabricated structures are very stable even under wet conditions, any HFIP residue could be further removed by washing with or immersing in deionized water. Third, for medical applications, the volatilized composites should be safe to cells or tissues in theory. In previous work, the chitin nanofiber-based structures prepared by this approach have been shown to be nontoxic to Schwann cells [35]. As demonstrated later in our study, the 293 T and NIH 3T3 cells can also proliferate well on the electrospun fiber samples. Taken together, the use of HFIP does require safety precautions, but the composite samples produced do not necessarily cause toxicity to the cells due to its volatility and easiness to remove.

The aforementioned CBD domain is designed to improve the intramolecular interaction between the protein and chitin molecules. Previous studies show that the CBD domains expressed by the *E. coli* BL21 (DE3) can fold into correct conformation and possess a good interaction with chitin through hydrophobic interaction [47,48]. Here, the native function of the CBD domain in the recombinant protein was confirmed by the Quartz crystal microbalance (QCM) analysis. As revealed, QCM curves showed that the chitin-coated chips could absorb more SPCC (7.97 ± 0.04 mg/m^2) and SNCC (6.71 ± 0.01 mg/m^2) compared to $_{Spytag}CsgA$ (3.08 ± 0.02 mg/m^2) and $_{Snooptag}CsgA$ (2.71 ± 0.02 mg/m^2), respectively (Figure S7), showing the functionality of the appended CBD domain in the proteins (Fig. 2h). When the components are dissolved in the HFIP solvent, both the protein and chitin components were denatured from their original conformations. However, unlike the chitin molecules, the protein samples could not recover their fibrous morphologies as well as their β-sheet structures after HFIP evaporation. To regain their nanofiber morphologies as well as β-sheet structures, we performed an additional methanol curing step. Similar to the curing protocol used for processing silk proteins [39,49], the β-sheet structure, as verified by ATR-FTIR spectra, and fiber morphology, revealed by AFM images, would recover

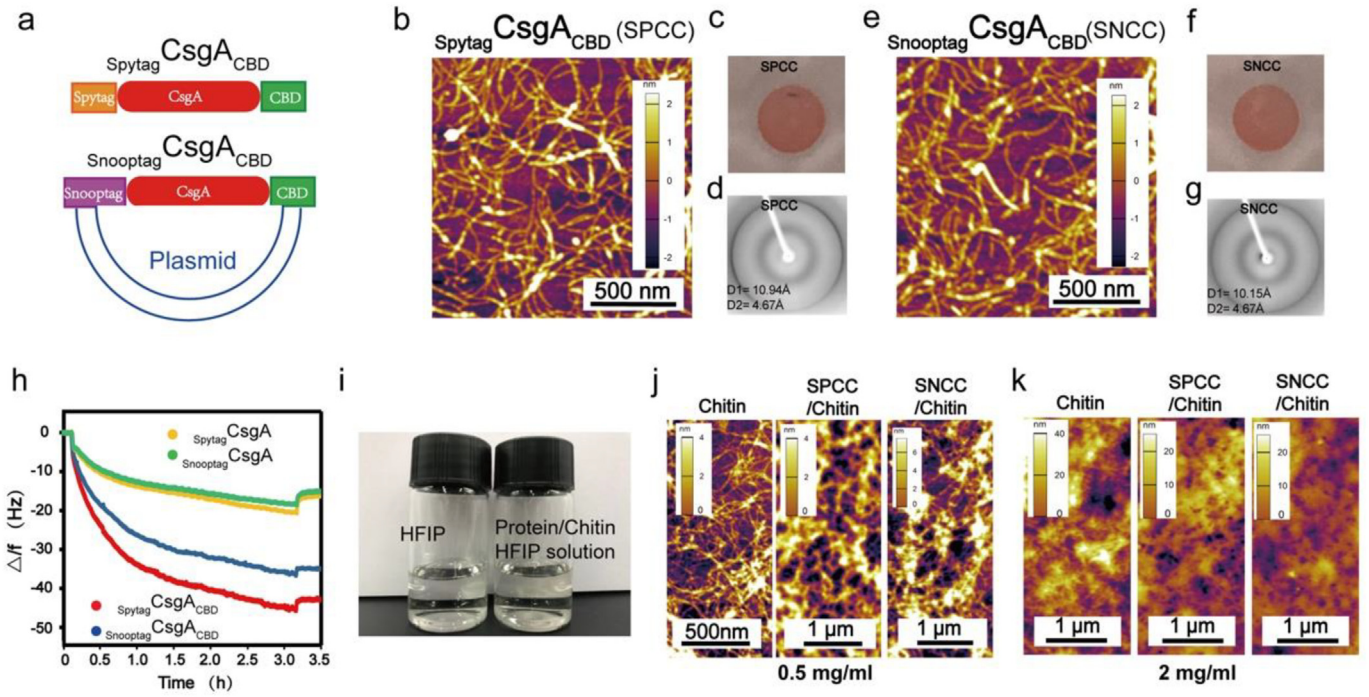

Fig. 2. The functional components and the hybrid ink. (a) Modular genetic design for the multi-domain amyloid components: $_{Spytag}CsgA_{CBD}$ (SPCC) and $_{Snooptag}CsgA_{CBD}$ (SNCC). (b) Atomic force microscopy (AFM) image of the recombinant SPCC (0.5 mg/ml). (c) Congo Red (CR) staining assay of the SPCC. (d) X-ray fibril diffraction pattern: (D1) and (D2) for SPCC. (e) Atomic force microscopy (AFM) image of the recombinant SNCC (0.5 mg/ml). (f) The Congo Red (CR) staining assay of the SNCC. (g) X-ray fibril diffraction pattern: (D1) and (D2) for SNCC. (h) QCM curves for the recombinant protein fibers on the chitin surface. (i) Chitin and amyloid solutions in HFIP. (j) The AFM topographic images of the chitin and amyloid/chitin hybrid ink dried on the mica sheets at a 0.5 mg/ml concentration. (k) The AFM topographic images of the chitin and amyloid/chitin hybrid ink dried on the mica sheets at a 2 mg/ml concentration.

with the help of methanol [30,49] (Figure S2). To verify if the functionality of the CBD domain would be regained from the HFIP treatment followed by methanol curing, we assessed and compared the mechanical properties of the produced composites before and after methanol curing. As revealed, the cured CsgA/chitin and $CsgA_{CBD}$/chitin composites both possessed a higher Young's modulus than their uncured counterparts and the cured $CsgA_{CBD}$/chitin (7.33 ± 0.013 GPa) mixture had higher modulus than both the cured CsgA/chitin (5.73 ± 0.019 GPa) and uncured $CsgA_{CBD}$/chitin (2.25 ± 0.010 GPa) composites, implying the strong interactions between the CBD domain in the $CsgA_{CBD}$ protein and chitin could be rescued after the methanol curing step (Figure S3, 4). In addition, compared with the cured CsgA/chitin composite prepared by an airbrushing approach, the $CsgA_{CBD}$/chitin sample more easily formed a free-standing film on the PDMS matrix under the same conditions (Figure S10). This result indicated that the presence of CBD domain might play a role in enhancing the cohesive force of the composites arising from the intermolecular interactions between the CBD domains and chitin.

After the methanol treatment process, the fibrous morphology of the chitin and amyloid-chitin composites was clearly evident as shown by the topographic images in Fig. 2i, and by the atomic force microscopy (AFM) analysis (Fig. 2j and k). The images in Fig. 2i show the chitin and hybrid fibers (chitin co-self-assembled with amyloid protein) at a concentration of 0.5 mg/ml. In contrast, the composites show no obvious fiber morphology at a concentration of 2 mg/ml (Fig. 2j), while hybrid fibers are still formed by chitin at this concentration. The morphology of the composites is also different from the protein fibers at the same concentration (Figure S8). These results show that the morphology of the dried amyloid-chitin composites varied with the concentration of the ink and that in higher concentration conditions no obvious fibrous structures were observed on the printed surfaces likely due to fiber aggregation as well as the AFM tip-sample convolution effects.

The HFIP solvent system enables the amyloid-chitin complexes to be applied by multiple fabrication methods, so we explored the potential of the hybrid ink to be fabricated into different structures using several different approaches. First, we tested the functionalities of the hybrid ink by simply dropping it into a methanol bath where it formed some ball-like structures. The amyloid-chitin composites were unable to dissolve in the methanol bath, while the HFIP dispersed in the methanol solution allowing the hybrid ink to be fixed into shapes. No obvious fiber structures were observed on the surface of these balls. To test the functionalities of these amyloid/chitin composite structures, we engineered fluorescent fusion versions of the SPCC and SNCC with $mCherry_{spycatcher}$ and $GFP_{snoopcatcher}$, respectively. These fluorescent variants were mixed with chitin as before and were able to form balls upon addition to methanol. Fluorescence microscopy revealed that the balls were fluorescent, demonstrating that SPCC and SNCC can be conjugated with $mCherry_{spycatcher}$ and $GFP_{snoopcatcher}$, respectively (Figure S5).

We showed that a hybrid ink composed of recombinant amyloid protein and chitin purified from a natural material can be fixed into simple shapes when the HFIP solvent is removed. We next investigated the possibility of applying the hybrid ink coupled with different fabrication methods followed by methanol curing to produce pre-defined or well-ordered structures.

3.3. Hybrid ink coupled with airbrushing for complex thin film fabrication

Airbrushing is a method to spray solutions as a vapor onto a template to get a thin coating or a film. Here, by taking the advantage of the rapid evaporation property of HFIP, we used airbrushing to fabricate our hybrid ink, which enabled a macro-level fabrication over a large area. Different concentrations of the hybrid ink were sprayed onto a PDMS-coated glass slides. When its concentrations were higher than 2 mg/ml, it became very sticky and was cured in several seconds when exposed to the air, so these concentrations are not suitable for airbrushing (Figure S9). However, suitable results were obtained when applied at 2 mg/ml (Fig. 3a). After airbrushing onto the template, the liquid accumulation allowed us to lift out a transparent freestanding film (Fig. 3b). At the same concentration, the CsgA-chitin ink was unable to effectively form a film, highlighting the novel property of the hybrid-proteins (Figure S10). A cross-section SEM image of the freestanding film (Fig. 3c) shows that the film thickness is about 3.5 μm (spray time 200s at a rate of 0.02 ml/s). Surface SEM (the upper picture on the righthand image) in Fig. 3c shows the unique fiber morphology on the surface of the freestanding film. The cross-section and zoom-in image show the multilayer structures inside the film (lower picture in righthand image) in Fig. 3c. To further characterize the relationship between the film thickness and spraying time, we carried out a series of experiments. The curve in Fig. 3d shows the film thickness varying with the spraying time in a nonlinear relationship. For thin film materials the optical properties, like transmittance and reflectivity, and mechanical strength are also affected by the film thickness. We then analyzed the optical properties of films prepared with spraying times of 100s, 200s, 400s and 800s.The curves in Fig. 3e show that the transmittance of all the samples is high, while their reflectivity is low. However, with increasing thickness of the film, the transmittance decreases, while the reflectivity increases.

Next, we picked two films of different thicknesses to test their mechanical properties. Fig. 3f shows the stress-strain curves of the two films. Here, we adopted the first stage of the stress-strain curves for the two films and applied the slope fitted for each curve to calculate the elastic modulus (Fig. 2f). The elastic modulus for the films is 0.68 ± 0.14 Gpa for the 10 μm thick film and 0.43 ± 0.08 Gpa for the 5 μm thick film. Differences in the elastic stage of the stress-strain curve were observed between the films and a non-linear relationship between the thickness and the spraying time was evident. This suggests that applying differing amounts of solution not only causes differences in thickness, but also affects the structures of the ink accumulating on the PDMS template. This indicates that tuning the technological parameters of the spraying can be used to obtain thin films with different physical properties.

Another approach to generate novel properties is to use the integrated Spytag/Snooptag sequences, which allow conjugation of other proteins, to further functionalize the composites. We used the SPCC/chitin ink to make a film and then conjugated the film with $mCherry_{spycatcher}$. The fluorescence microscope image in Fig. 3g shows the red fluorescent signal resulting from the $mCherry_{spycatcher}$ conjugates. To further expand the functionality of our amyloid-chitin composite materials, we next tested whether the composite films could be functionalized with enzymes to catalyze the degradation of organophosphate pesticides. We chose a single enzyme, organophosphate hydrolase (OPH) [51], which can catalyze the degradation of the pesticide paraoxon (PAR) into a less harmful intermediate product para-nitrophenol (PNP). PNP has a strong absorption intensity at 405 nm, enabling us to easily monitor the formation of reaction products. We constructed, recombinantly produced, and purified an $OPH_{spycatcher}$ fusion protein with a good activity (Figure S11) and then conjugated it to a SPCC/chitin film. In Fig. 3h, the schematic shows the Spycatcher engineered enzyme conjugated with the amyloid fibers in the composite film. A $CsgA_{CBD}$/chitin composite film was also exposed to $OPH_{spycatcher}$ as a control. After a 0.5 h reaction, the unconjugated fusion enzymes were washed away. Whereas our PAR-degradation assays revealed time-dependent increases in absorption intensity at the 405 nm wavelength for the SPCC/chitin films, at the same time, almost no catalytic activity was detected for the $CsgA_{CBD}$/chitin composite film (Fig. 3h). Collectively, our results show that by altering the fabrication parameters we can get a series of thin films with different properties, at the same time, these films can also be functionalized by fusing other protein domains via genetic engineering.

3.4. Hybrid ink coupled with electrospinning for fabrication of fibrous webs

Electrospinning techniques can be used to fabricate diverse fibers and other complex structures [52] that exhibit a variety of unique properties, including high porosity, good mechanical strength, large surface area per

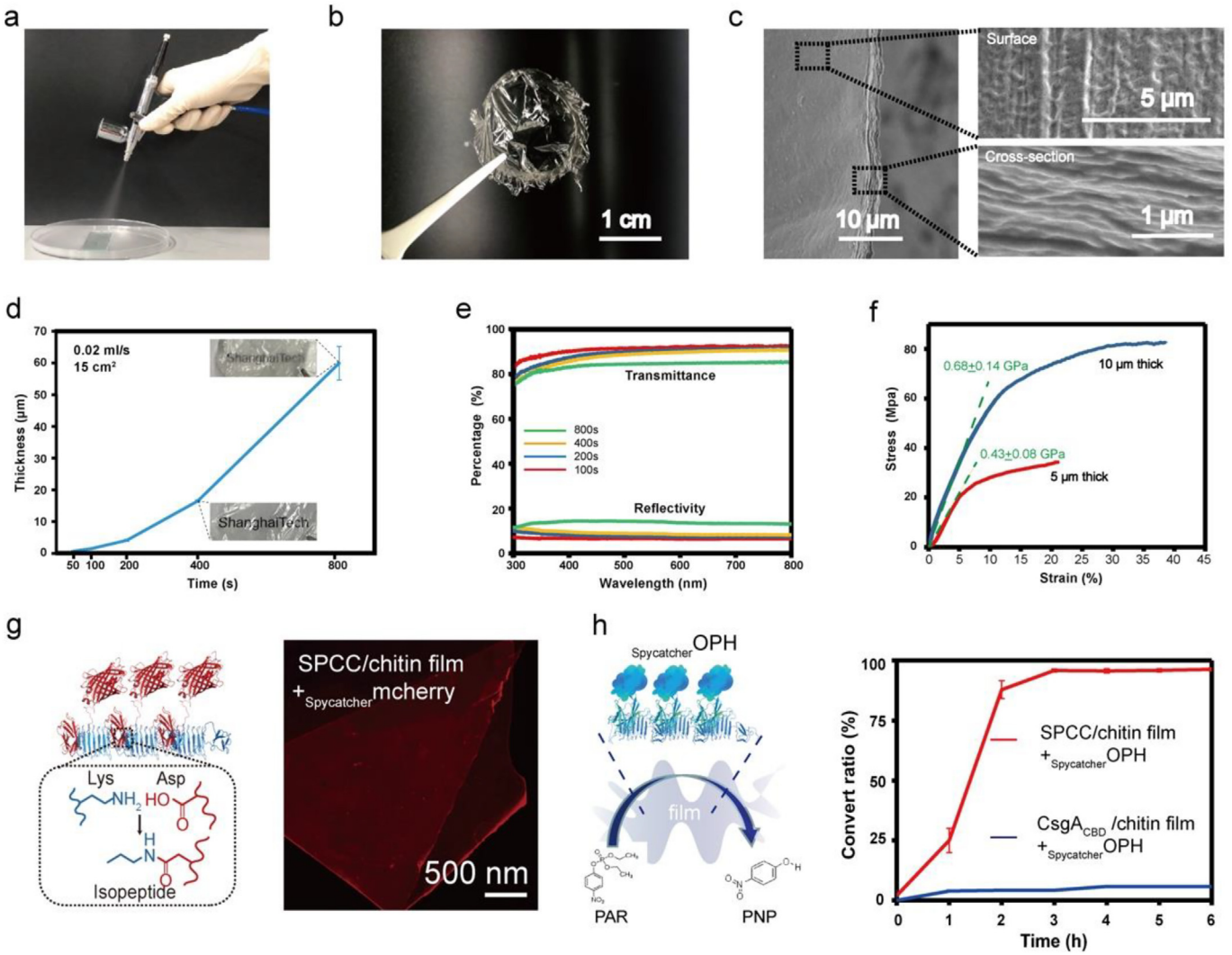

Fig. 3. The amyloid-chitin hybrid ink coupled with airbrushing to produce thin film structures. (a) Setup for the hybrid ink airbrushing using a commercially available tool with a 15° spray angle. (b) Airbrushed transparent film (200s, 2 mg/ml) lifted out from a petri dish mold. (c) A SEM image of the airbrushed film with a thickness of about 3.5 μm. The two SEM images on the right show the surface morphologies (upper picture) and the cross-section (lower picture) of the film in (c). (d) The curve shows the trend of the thickness varies with the spraying time. (e) The transmittance spectra of airbrushed films of different thickness. (f) The stress-strain curves of airbrushed films with different thickness, and the fitting slope applied for calculating the elastic modulus of the films. (g) The cartoon on the left shows how the spytag and spycatcher conjugate with each other. A fluorescence microscope image showing the red fluorescence of the airbrushed film made from SPCC/chitin film conjugated with $mCherry_{spycatcher}$. (h) The cartoon on the left shows immobilization of the $OPH_{spycatcher}$ on the airbrushed film made from SPCC/chitin hybrid ink. The curves on the right show the conversion ratio of the paraoxon by the two different film systems ($OPH_{spycatcher}$ conjugated with SPCC/chitin film and $OPH_{spycatcher}$ conjugated with $CsgA_{CBD}$/Chitin film).

unit mass, and high gas permeability, among others [53]. Notable applications of fibers fabricated through electrospinning including membrane filtration, catalytic processes, fibrous-sensor applications, drug delivery, and tissue engineering [54–56]. We thus investigated the potential of using electrospinning to prepare fiber webs from our amyloid/chitin composite ink.

We began by testing different conditions to optimize fiber formation (Figure S13). We found that to obtain amyloid/chitin fiber webs the chitin component must be at a high ratio (Figure S14 a). We then explored how other parameters affected the fiber morphologies using a fixed chitin concentration (Figure S14 b c d and Figure S15). The results reveal that the electrospinning fiber webs can be prepared with different sizes by altering the parameters. We mainly used SEM to observe these electrospinning fibers or count the fiber diameters, at a view of one to one hundred micrometers. The SEM image in Fig. 5a shows the electrospinning fibers of SPCC/chitin, with the following conditions: voltage 15kv, distance 15 cm, flow rate 0.05 ml/min and an inner needle diameter 0.5 mm. The fiber diameter is about 0.14 ±0.03 μm. The SEM image in Fig. 4a shows the morphology of the amyloid/chitin electrospun fiber webs. The webs could be lifted out of the collecting matrix (Fig. 4b). The SEM image in Fig. 4c shows the details of the fiber film produced by electrospinning. The film surface and cross-sections both show a fiber web morphology. To demonstrate the functionalization of the electrospun fiber webs, the SPCC/chitin and SNCC/chitin electrospun fibers were conjugated with $mCherry_{spycatcher}$ and $GFP_{snoopcatcher}$, respectively, and observed with fluorescence microscopy (Fig. 4d). In addition to Spytag and Snooptag, the His-tag on the C-termini of our protein sequences is another functional site. Previous work has shown that binding with nanoparticles in a precise and highly ordered manner can generate materials that are highly suitable for applications in bio-photonics and bioelectronics. Specifically, nitrilotriacetic acid (NTA) decorated QDs can be attached to a protein component via molecular recognition in "NTA-Metal-His" coordination chemistry. Our group previously demonstrated the functionalization of genetically modified biofilm fibers with this type

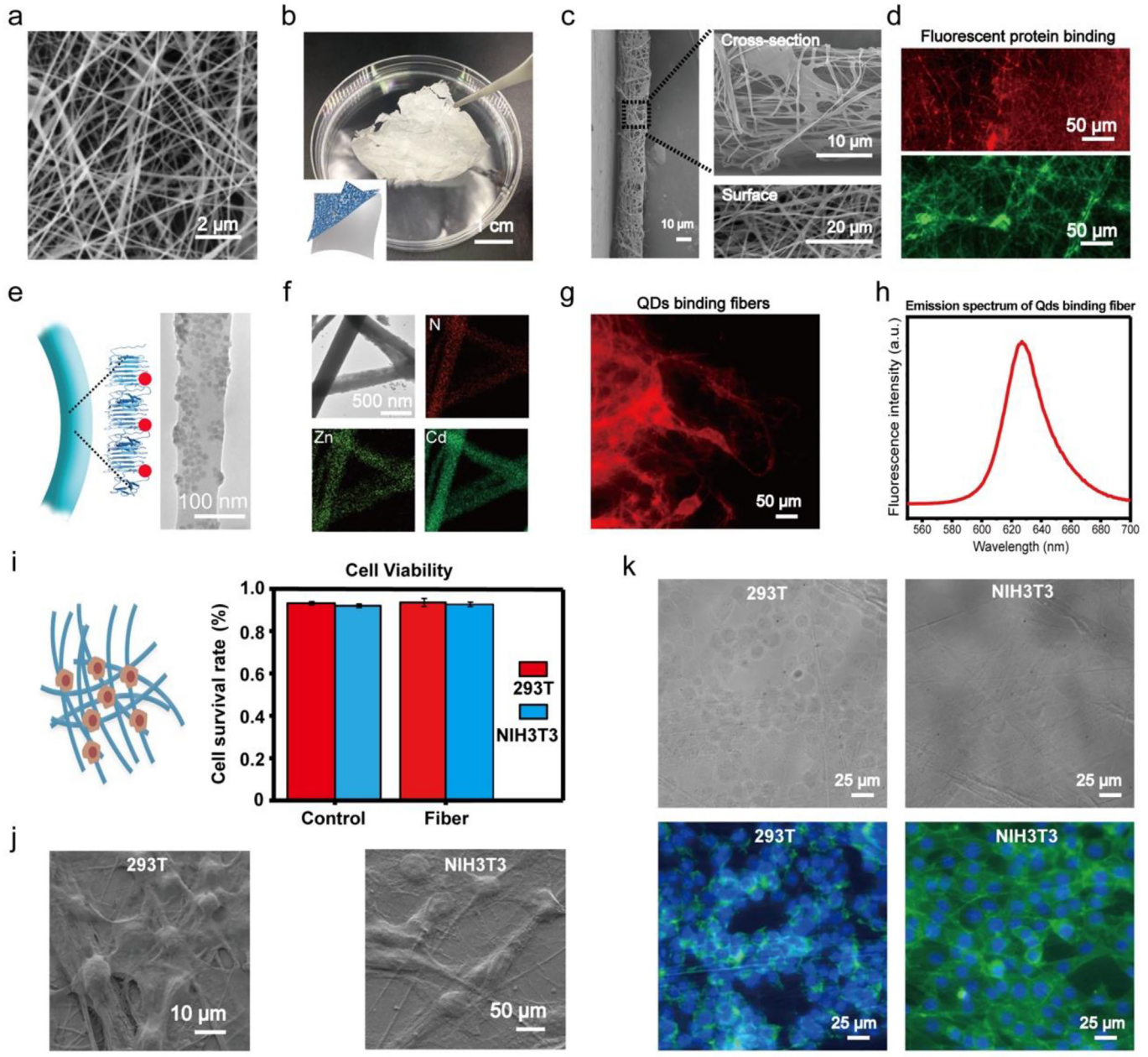

Fig. 4. The amyloid-chitin hybrid ink coupled with electrospinning to produce fiber webs. (a) Electrospun fiber webs. (b) A freestanding electrospun fiber web film. (c) The SEM images show cross-section and surface morphologies of the freestanding electrospun fiber web film. (d) Fluorescence microscope images showing the red and green fluorescence of the electrospun fiber webs made from SPCC/chitin and SNCC/chitin electrospun fiber webs conjugated separately with $mCherry_{spycatcher}$ and $GFP_{snoopcatcher}$. (e) Schematic showing the electrospun fiber conjugated with quantum dots (QDs) (left) and a TEM image showing the binding of QDs to fibers (right). (f) EDS (Energy Dispersive Spectrometer) mapping images of the corresponding elements for the SEM image version. (g) Fluorescence microscopy image showing the red fluorescence of the electrospun fiber functionalization with the red-emitting QDs (CdSeS@ZnS QDs). (h) The CdSeS@ZnS photoluminescence spectrum of the QD arrays on the electrospun fibers. (i) Schematic showing cells grown on the electrospun fiber webs. The quantitative trypan blue counting assay showing the viability of the HEK293T and NIH3T3 after a standard proliferation period; measurements are the average of triplicate cultures. (j) The SEM images showing the cells maintain a good interaction with the electrospun fiber webs. (k) Bright field and fluorescence overlay images showing that the HEK293T cells and NIH3T3 cells can grow normally on the electrospun fiber webs.

of QDs [57]. With the aim of using the poly-histidine tag on the C-terminal of the fusion amyloid proteins to generate an ordered array of inorganic nanoparticles in a spatially controlled manner (Fig. 5e cartoon), we tested SPCC/chitin and SNCC/chitin with NTA-modified CdSeS@ZnS QDs as previously decribed [49]. TEM revealed the QDs were well-arrayed on the fibers (righthand image, Fig. 4e), but the chitin fibers were unable to conjugate with the QDs (Figure S16). On the other hand, fluorescence microscopy showed fluorescent QDs on the composite fiber webs produced by electrospinning, and the fluorescence emission spectra confirmed the presence of characteristic signals from the QDs on the fibers (Fig. 4g and h). We also performed EDS element mapping to assess the distribution of elements for the QD-functionalized fibers: N signals detected represent the biomass component, Zn and Cd signals represent the CdSeS@ZnS QDs (Fig. 4f). The TEM morphological characterization, the fluorescence spectrum, and the EDS mapping all confirm that the QDs are attached to the amyloid/chitin electrospun fibers.

The extracellular CsgA secreted by pathogenic bacteria such as *E. coli*, can bind to proteins present on host cells. We speculated that the unique

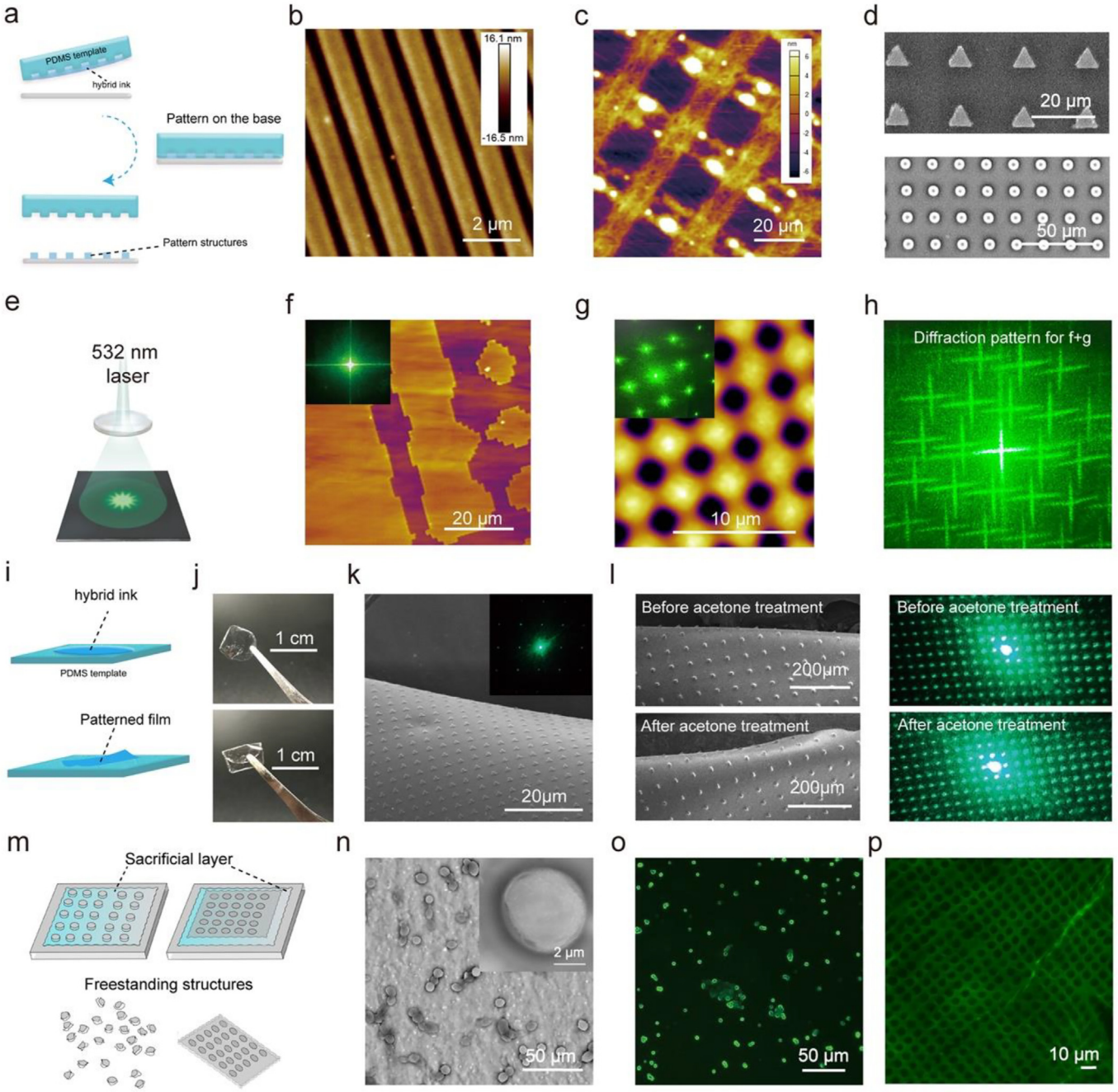

Fig. 5. The amyloid-chitin hybrid ink coupled with soft-lithography can be used to produce pattern structures. (a) The fabrication process of the film-based pattern structures. (b) The fabrication process of the film-based pattern structures. (c) The cross-bar pattern fabricated by the hybrid ink. (d) The pattern arrays fabricated by the hybrid ink. The upper image shows a triangle array and the bottom image shows a dot array. (e) Pattern structures for use in directing light-paths. (f) Film-based pattern structures and the associated light diffraction pattern (inset image). (g) Another structure made by the same method. The inset image shows the associated diffraction pattern. (h) The image shows the synthesis pattern (f + g). (i) The fabrication process for the freestanding photonic device. (j) The patterned freestanding photonic device and the folded device. (k) The SEM image of the freestanding photonic film after being folded 100 times and the associated diffraction pattern. (l) The SEM images show the freestanding photonic film before and after acetone treatment. (m) The fabrication process for the freestanding dots and porous sheets. (n) The freestanding dots. The right-up corner image shows a zoom-in picture of a dot. (o) The fluorescence microscope image shows the freestanding composite dots conjugated with $GFP_{snoopcatcher}$ made by SNCC/chitin. (p) The fluorescence microscope image shows the freestanding composite porous sheet conjugated with $GFP_{snoopcatcher}$ made by SNCC/chitin.

fiber web structures formed by the amyloid and chitin components may mimic the extracellular matrix (ECM) and facilitate cell adhesion to the electrospun fibers. In this case, the electrospun fiber webs may serve as a suitable matrix for cellular growth. To test this idea, we observed the cell morphology of human embryonic kidney cells (HEK 293 T) and mouse embryonic fibroblast cells (NIH 3T3) cultured the on the electrospun fiber webs. Morphological characterization by SEM revealed that both cell types could attach to the electrospun fibers (Fig. 4j), indicating a good interaction between the cells and the fiber webs. Fluorescence microscopy showed that the cells had normal shaped cytoskeletons and nuclei (Fig. 4k). At the same time, the viability of the cells growing on the electrospun fibers did not differ from that of cells grown in a standard petri dish culture (Fig. 4i). These results show that the electrospun fiber webs can be used like a biomimetic ECM matrix for cell culture.

3.5. Softlithography-based fabrication of amyloid-chitin composites for detailed structures

Having demonstrated the fabrication of our amyloid-chitin composites at the macro-level, we next used soft lithography to produce finely ordered structures at the micro-meter level. Specifically, we used a micro transfer molding process with PDMS stamping. The features on the silicon wafer were replicated by PDMS, and these PDMS molds were used as the template for pattern forming. By altering the molds, we produced a series of structures which differed in size and shape. By altering the base matrix or the fabrication method, we could produce film-based patterns, freestanding patterns or freestanding films with micro-level pattern structures. The cartoon in Fig. 5a shows the fabrication process for the film-based pattern structures. Using this approach, a simple straight-line pattern was fabricated on a glass sheet. The AFM image in Fig. 5b shows the micro-structures for this pattern structure. Except for the two-component ink, the components can be fabricated separately. In Fig. 5c, a cross-bar pattern is shown that was fabricated by a layer-by-layer method. The first layer was fabricated by the chitin ink and the amyloid ink was perpendicularly patterned on the chitin structures. In addition to these large structures, we also fabricated repeat arrays. We fabricated two repeat arrays: triangles and dots. The SEM images in Fig. 5d show these structures in detail (triangle pattern in the upper picture; dot pattern in the lower picture). These organized structures can direct the light-path to form diffraction patterns. The diffraction patterns were produced when the light went through these structures depending on the morphology and scale of the structures. The cartoon in Fig. 5e shows the potential application of this technology in a photonic device, as a light guiding grating. The AFM images in Fig. 5f and g show the micro pattern structures for two different gratings and their diffraction patterns (inset image). For these two structures, the diffraction pattern was synthesized by directing a laser through the gratings. The image in Fig. 5h shows the diffraction pattern when the light first went through one grating (Fig. 5f) then through the second grating (Fig. 5g). In addition to these film-based gratings, we also fabricated freestanding patterned films. Fig. 5i shows the fabrication process for the freestanding gratings. The hybrid ink is dried on the patterned PDMS template and then the patterned film can be lifted from the template. In Fig. 5j, we can see images of the transparent grating and how this patterned film can be folded. The SEM image shows that the micro level structures were intact with a good diffraction pattern after being folded 100 times (Fig. 5k). Unlike traditional synthesized polymers which can be dissolved by organic solvents, the composites can resist solvents such as acetone. The SEM images in Figure 5l show the micro pattern structures before and after acetone treatment. These structures were not affected by acetone and the grating still was able to display good diffraction patterns (Figure 5l). In addition to freestanding films, we also produced freestanding structures by fabricating our pattern structures on a water-soluble sacrificial layer. Here the hybrid amyloid-chitin ink was patterned on a water-soluble polyvinyl alcohol (PVA) layer and cured by methanol steam. Since the PVA matrix was water soluble but our patterns were not, the PVA layer were removed using water to produce freestanding structures (Figure 5m). We fabricated dot arrays with the same template in Fig. 4d on a PVA layer and then dissolved the PVA matrix. In Figure 5n the SEM images show the freestanding dots (the inset image is a zoom-in picture of one dot). The dot diameter is initially about 6.25 ± 0.15 μm (Fig. 5a), but SEM analysis revealed that the diameter of the dots shrinks by about 2 μm after removing the PVA base layer. We then made the dot arrays by SNCC/chitin hybrid ink, and fluorescence caused by $GFP_{snoopcatcher}$ conjugation could be observed in the dots (Figure 5o). In addition to freestanding dots, we also produced a freestanding porous sheet structure. Figure 5p shows a fluorescence microscope image of a freestanding porous sheet of an SNCC/chitin $GFP_{snoopcatcher}$ conjugation with a 5 μm diameter porosity. A 10 μm diameter porous sheet was also fabricated (Figure S12). We were able to tune the parameters of these structures by altering the mold or the component ratio of the ink. Changes in protein content affected the conjugation of fluorescent proteins as indicated by the different fluorescence intensities.

In summary, we were able to easily fabricate well-ordered micro or nano level structures, with potential applications in photonics and biomedicine, using our biomolecule-based ink system.

4. Conclusion

We have developed a hybrid ink that contains two components, genetically programmable self-assembling amyloid protein and chitin, the second most abundant polysaccharide in nature. Using our hybrid ink system, these two biomacromolecules can be easily fabricated into desired structures and shapes. In addition to the fabrication methods demonstrated here, some other fabrication methods may also be compatible with our hybrid ink, such as electro-spraying [38], 3D printing [36], particle replication in nonwetting templates (PRINT) [58], electron beam lithography [59], nanoimprint lithography [60] and so on. Through these technologies this ink can be shaped into diverse well-defined structures with broad potential applications across fields. For now, we have shown it can be used to create freestanding films, dots, photonic grating and micro-fibers, and we have demonstrated the functional potential of its multiple binding sites for some simple applications. By engineering its catalytic functions, the film could be used in food packaging or for the degradation of toxins on surfaces. The chitin-based ECM-like electrospun fiber webs have great potential in tissue culture applications, including tissue engineering. Given the possibility of further functionalization, the free-standing dots can be utilized for diverse medical applications. For example, if some antigen peptide sequences are incorporated to the protein component, the dots having specific interactions with the immune cells can be applied as vaccine or an immunotherapeutic carrier for cancer treatment [61,62]. In addition, a drug delivery system can also be developed based on these dots [63] either by genetically engineering of certain therapeutic peptide sequences or through chemical conjugation of drug molecules on the protein components [64]. For the photonic grating patterns, more complex light-guiding structures could be fabricated to fulfill broad applications such as anti-reflection, environmental sensing or photonic electrodes.

Peptides possessing unique functionalities have already been applied in materials science. Our study extends these potential applications based on the ability to genetically engineer different functionalities into the amyloid component of a hybrid mixture to create a genetically programmable ink. Indeed, diverse amyloid-polysaccharide composites with tunable functions and shapes could be fabricated using this programmable ink, leading to applications ranging from biocatalysis, cell scaffolding and biophotonics. We anticipate that our work will spur further efforts in exploring genetically engineered proteins and their complex structures for biofabrication and application in multiple fields.

Author's contributions

Shicao Wei: Conceptualization, Formal analysis, Investigation, Writing- Original Draft. Yingfeng Li: Resources. Ke Li: Resources, Anqi Kang: Resources, Siyu Zhang: Resources. Feng Teng: Resources. Hui Zhang: Resources. Chao Zhong: Conceptualization, Methodology, Writing-Reviewing and Editing, Supervision.

Declaration of competing interest

The authors declare that they have no known competing financial interests or personal relationships that could have appeared to influence the work reported in this paper.

Acknowledgements

The AFM characterization were executed at the Analytical Instrumentation Center (AIC), SEM and TEM work is supported by the Center

for High-resolution Electro Microscopy (ChEM) at Shanghai Tech University. The authors thank Dr. Xinyan Wang for AFM training, Dr. Weiyan Liu, Yilan Jiang for TEM and SEM training, Kaimin Xu for TEM characterization. This work was sponsored by the National Key R&D Program of China (grant nos. 2018YFA0902804 and 2020YFA0908100, the two grants provide equal support), the Joint Funds of the National Natural Science Foundation of China (key program no. U1932204).

Appendix A. Supplementary data

Supplementary data to this article can be found online at https://doi.org/10.1016/j.mtbio.2021.100179.

References

[1] C. Ortiz, M.C. Boyce, Science 319 (5866) (2008) 1053.
[2] U.G. Wegst, et al., Nat. Mater. 14 (1) (2015) 23.
[3] M.A. Meyers, et al., Science 339 (6121) (2013) 773.
[4] U.G. Wegst, et al., Nat. Mater. 14 (1) (2015) 23.
[5] C. Sanchez, et al., Nat. Mater. 4 (4) (2005) 277.
[6] S. Ling, et al., Nat. Rev. Mater. 3 (2018) 18016.
[7] M. Eder, et al., Science 362 (6414) (2018) 543.
[8] P.-Y. Chen, et al., Acta Biomater. 4 (3) (2008) 587.
[9] S. De Baets, et al., Polysaccharides II: Polysaccharides of Eukaryotes, Chemical Industry Press, 2004.
[11] M.K. Jang, et al., J. Polym. Sci. Part A Polymer Chemistry 42 (14) (2004) 3423.
[12] C.M. Rufo, et al., Nat. Chem. 6 (4) (2014) 303.
[13] Z. Zhou, et al., Adv. Mater. 29 (15) (2017) 1605471.
[14] J. Jin, et al., Adv. Mater. 28 (26) (2016) 5169.
[15] C. Li, et al., Adv. Mater. 26 (20) (2014) 3207.
[16] R. Jayakumar, et al., Biotechnol. Adv. 29 (3) (2011) 322.
[17] P. Mohammadi, et al., Sci. Adv. 5 (9) (2019) eaaw2541.
[18] J. Jin, et al., Adv. Mater. 25 (32) (2013) 4482.
[19] J.G. Fernandez, D.E. Ingber, Adv. Mater. 24 (4) (2012) 480.
[20] H. Kweon, et al., J. Appl. Polym. Sci. 80 (7) (2001) 928.
[21] Y. Zhao, et al., ACS Omega 2 (11) (2017) 7471.
[22] I. Drachuk, et al., Acs Biomaterials Science & Engineering, 2017 acsbiomaterials.7b00367.
[23] Y. Yuan, et al., J. Agric. Food Chem. 62 (19) (2012) 4434.
[24] J.-M. Malho, et al., Chem. Commun. 50 (55) (2014) 7348.
[25] M.M. Barnhart, M.R. Chapman, Annu. Rev. Microbiol. 60 (1) (2006) 131.
[26] P.Q. Nguyen, et al., Nat. Commun. 5 (1) (2014) 1.
[27] C. Zhong, et al., Nat. Nanotechnol. 9 (10) (2014) 858.
[28] M. Cui, et al., Chem. Sci. 10 (14) (2019) 4004.
[29] Y. Wang, et al., J. Mol. Biol. 430 (20) (2018) 3720.
[30] Y. Li, et al., Nano Lett. 19 (12) (2019) 8399.
[31] J.L. Shamshina, et al., ACS Sustain. Chem. Eng. 7 (7) (2019) 6444.
[32] C. Zhong, et al., Adv. Mater. 23 (41) (2011) 4776.
[33] A.M. Salaberria, et al., Eur. Polym. J. 68 (2015) 503.
[34] A. Cooper, et al., J. Mater. Chem. 22 (7) (2012) 3105.
[35] Z. Chao, et al., Soft Matter 6 (21) (2010) 5298.
[36] S.H. Kim, et al., Nat. Commun. 9 (1) (2018) 1.
[37] Y. Loo, et al., Nano Lett. 15 (10) (2015) 6919.
[38] D. An, et al., Nat. Commun. 7 (1) (2016) 1.
[39] H. Kweon, et al., Polymer 41 (20) (2000) 7361.
[40] X. Wang, et al., Adv. Mater. 30 (16) (2018) 1705968.
[41] F.S. Ruggeri, et al., Angew. Chem. Int. Ed. (2015).
[42] J. Adamcik, et al., Nanoscale 4 (15) (2012) 4426.
[43] S.C. Reddington, M. Howarth, Curr. Opin. Chem. Biol. 29 (2015) 94.
[44] G. Veggiani, et al., Proc. Natl. Acad. Sci. Unit. States Am. 113 (5) (2016) 1202.
[45] T. Ikegami, J. Biol. Chem. 275 (18) (2000) 13654.
[46] Y. Marcus, J. Solut. Chem. 20 (9) (1991) 929.
[47] M. Hashimoto, et al., J. Bacteriol. 182 (11) (2000) 3045.
[48] S. Ferrandon, Biochim. Biophys. Acta Gen. Subj. 1621 (1) (2003) 31.
[49] H.Y. Kweon, Y.H. Park, J. Appl. Polym. Sci. 73 (14) (1999) 2887.
[51] H.D. Lu, et al., Protein Eng. Des. Sel. 23 (7) (2010) 559.
[52] J. Doshi, D.H. Reneker, J. Electrost. 35 (2–3) (1995) 151.
[53] C. Drosou, et al., Food Hydrocolloids 77 (2018) 726.
[54] D.B. Khadka, D.T. Haynie, Nanomed. Nanotechnol. Biol. Med. 8 (8) (2012) 1242.
[55] L. Min, et al., Composites Communications 11 (2019) 12.
[56] S.Y. Chew, et al., Biomacromolecules 6 (4) (2005) 2017.
[57] X Wang, et al., Adv. Mater. 30 (16) 1705968.1.
[58] J. Xu, et al., Angew. Chem. Int. Ed. 52 (26) (2013) 6580.
[59] X. Wu, et al., ACS Macro Lett. 8 (10) (2019) 1252.
[60] F. Dundar Arisoy, et al., ACS Appl. Mater. Interfaces 10 (23) (2018) 20055.
[61] R. Kuai, et al., Nat. Mater. 16 (4) (2016) 489.
[62] S.W. Metz, et al., PLoS Neglected Trop. Dis. 10 (10) (2016), e0005071.
[63] K. Khodabandehlou, et al., Advanced Healthcare Materials 5 (6) (2016) 653.
[64] Zasloff, Michael, Nature 415 (6870) (2002) 389.
[66] Li Yingfeng, et al., Sci. Adv. 6 (21) (2020) eaba1425.
[67] Yanyi Wang, et al., Nat. Chem. Biol. 17 (3) (2021) 351.
[68] Bolin An, et al., Matter 3 (6) (2020) 2080.
[69] J Pu, et al., Adv. Sci. 7 (14) (2020) 1903558.